JACS Au
AN OPEN ACCESS JOURNAL OF THE AMERICAN CHEMICAL SOCIETY

pubs.acs.org/jacsau
Article

Solvent Reorganization in Stabilized Protein–Polymer Conjugates Visualized by Two-Dimensional Infrared and Nuclear Magnetic Resonance Spectroscopy

Raiza Maia,[†] Xiaobing Chen,[†] Emma Mulry, Matthew T. Eddy,* and Carlos R. Baiz*

Cite This: *JACS Au* 2026, 6, 1801–1811

ABSTRACT: PEGylation is essential for the effective function of biologics, shielding them from rapid degradation and clearance in the complex environment of the human body. Despite its significance, a mechanistic understanding of PEGylation's role in enhancing protein stability is incomplete, limiting the ability to design PEGylated proteins with predictable properties. Solvation, a well-known driving force in protein folding and stability, is hypothesized to play a central role in protein stabilization via PEGylation, but molecular mechanisms underlying solvent-driven stabilization are not well understood. Here, we investigated solvent dynamics and the interactions of the solvent with the PEGylated carbohydrate recognition domain of human Galectin-3 (Gal3C) in aqueous solutions. Two-dimensional infrared (2D IR) spectroscopy, which captures subpicosecond molecular ensembles, revealed polymer length-dependent differences in protein dynamics and solvent dynamics for PEGylated Gal3C. Slower solvent dynamics correlated with increased conjugate thermal stability. Complementing these data, multidimensional nuclear magnetic resonance (NMR) spectroscopy provided evidence that Gal3C conjugated to longer PEG forms a noncovalent interaction "shroud", which correlated with changes in dynamics of the solvent and protein backbone. Molecular dynamics (MD) simulations supported an interpretation of the experimental results that PEGylation did not reduce the protein's solvent-accessible surface area. The integration of these data challenges the idea that PEGylation stabilizes conjugated proteins by dehydrating a protein's surface. Instead, these data support a mechanism where PEGylation improves protein stability by stabilizing the protein's solvation shell. These insights offer guidance for optimizing polymer length to achieve the desired thermal stability in biologics.

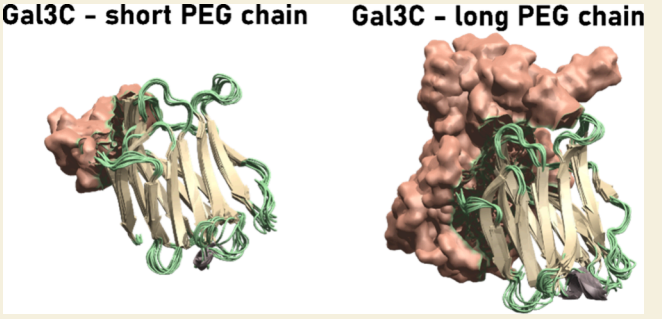

KEYWORDS: *Galectin-3, PEGylation, protein solvation, conformational changes, NMR spectroscopy, 2D IR, MD simulations*

INTRODUCTION

Biologics are one of the fastest-growing sectors in the pharmaceutical industry,[1,2] accounting for over 40% of all FDA-approved oncology drugs from 2000 to 2022 and have predominant roles in the development of biomarkers and many other disease treatments.[3] However, the molecular complexity driving their target specificity also makes biologics more vulnerable and less robust than small molecules. One of the most promising approaches to improving the stability of biologics is chemical conjugation with polymers, particularly poly(ethylene glycol) (PEG), to form protein–polymer conjugates.[4,5] While PEGylation has been shown to improve pharmacokinetic properties and prolong therapeutic efficacy of biologics,[6−11] its effects on protein stability and activity have been unpredictable, with studies reporting both an improvement and reduction in stability.[12−15]

The goal of obtaining mechanistic insight into how PEGylation alters protein properties has motivated extensive biophysical investigations of PEG-protein conjugates, with much of this work focused on defining the conformations of the protein and polymer within the conjugated system. Structural studies of crystallized PEGylated plastocyanin, together with nuclear magnetic resonance (NMR) characterization of its solution conformation, concluded that the polymer and protein behave largely as independent molecular entities, with limited direct interactions.[16] Solid-state NMR investigations of PEGylated proteins in sedimented solids similarly reported that the structures of PEGylated soluble proteins closely resemble those of microcrystalline preparations of the corresponding unmodified proteins.[17] Scattering-based approaches have also been applied to probe the global conformations of PEG and protein within conjugates, although

Received: December 12, 2025
Revised: February 3, 2026
Accepted: February 19, 2026
Published: February 25, 2026

https://doi.org/10.1021/jacsau.5c01692
JACS Au 2026, 6, 1801–1811

these studies have yielded differing conclusions regarding the extent of protein−polymer interactions.[18−21]

Here, we combine two-dimensional infrared (2D IR) spectroscopy, multidimensional NMR spectroscopy and NMR-based diffusion measurement, and molecular dynamics (MD) simulations to investigate the molecular mechanisms of protein−polymer interactions. Our work focuses on the role of the solvent and on how PEGylation modifies solvent−protein interactions and, in turn, macromolecular properties of PEGylated proteins. The application of 2D IR to protein−polymer conjugates complements prior approaches by enabling direct access to ultrafast molecular processes, allowing interrogation of protein−solvent interactions, solvent exposure, and the dynamics and organization of solvation networks surrounding proteins.[22] Experimental measurements on the picosecond to nanosecond time scales are especially valuable because they can be directly compared with MD simulations performed on comparable time scales, providing critical benchmarks for validating and extending computational models to additional systems of interest.[9−13,23] Solvent interactions with proteins are well-known to be among the most important driving forces in protein folding and unfolding.[24−28] In line with this view, growing evidence suggests that PEGylation enhances the thermal stability of conjugated proteins by modifying the solvation network surrounding the protein and altering its solvent-accessible surface area (SASA).[29] Computational simulations with PEGylated polypeptides and small proteins observed that a PEGylation-driven increase in protein stability correlated with a reduction in SASA.[30,31] For example, a combined experimental and computational study of a PEGylated small protein Pin1 indicated that PEGylation increased the disorder of water molecules in the protein solvation shell.[32] Coupled to this is the related question of the extent of interaction between the protein and polymer and how the two are spatially organized. In general, two models are frequently invoked to describe PEG-protein interactions: the "dumbbell model" and the "shroud model." These models differ in the extent of interaction between the protein and conjugated polymer. In the dumbbell model, PEG acts as a flexible polymer covalentely attached to the protein, while the majority of the chain remains extended and dynamic in solution. In this model, the protein and the PEG chain behave like two connected but distinct units, resembling the ends of a dumbbell (Figure 1). It is expected that the PEG primarily contributes steric bulk and excluded volume, modulating intermolecular interactions and crowding without strong interactions with the protein surface.[18−21] In contrast, the shroud model describes PEG as forming a more compact, surface-associated layer around the protein. In this case, the polymer samples conformations that keep it in close proximity to the protein surface, with the possibility of effectively creating a dynamic, hydrated protective layer. Overall, the "shroud" shields the protein from its environment, altering solvent access, intermolecular contacts, and surface interactions.[23,33,34] Real PEG-protein conjugates are expected to exhibit features of both, with the balance depending on chain length, grafting density, protein fold and surface polarity, and solvent conditions.

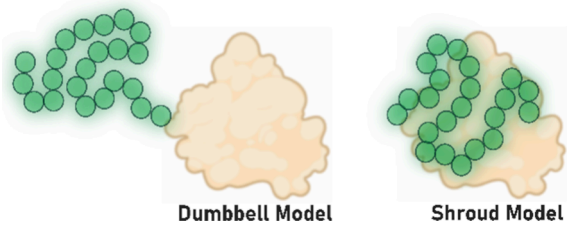

Figure 1. In the dumbbell model, the PEG chain is attached at a specific site on the protein but extends outward into solution, so the protein and the mobile polymer behave like two connected yet distinct units. In the shroud model, the PEG chain remains closely associated with the protein surface.

We hypothesize that the more extensive protein−polymer interactions in the shroud model have a greater impact on the protein's solvation network, thereby conferring greater stability to the conjugated protein. To test this hypothesis, we studied the dynamics and solvent interactions of the PEGylated carbohydrate recognition domain of human Galectin-3 (Gal3C), a human β-galactoside-binding lectin that plays a significant role in cell adhesion[35] and potentially in cancer biology.[36,37] Gal3C adopts a β-sandwhich structural motif, a widely observed motif found across different proteins. Based on databases that catalogue the frequency of all folds observed in experimentally determined protein structures,[38−40] it is estimated that approximately 10% to 20% of experimentally determined structures contained in the Protein Data Bank (PDB: 4R9C) exist as a β-sandwhich motif or contain domains formed by a β-sandwhich motif. As there are currently approximately 250,000 experimentally determined structures in the PDB, a conservative estimate would thus be approximately 25,000 of these contain β-sandwhich motifs. Further, proteins containing this fold are also highly significant in biology and medicine, including immunoglobulin and immunoglobulin-like domains found in antibodies, cell-surface coreceptors, receptor tyrosine kinases, growth factor receptors, and other medically relevant proteins, supporting the use of Gal3C as a representative model system.

Our investigation compared Gal3C conjugated with PEG molecules of two different molecular weights, 550 Da and 5 kDa, to investigate the relationship between the conjugated polymer and properties of the conjugated protein. Combining data from 2D IR spectroscopy, NMR spectroscopy, and molecular dynamics (MD) simulations, we compared the impact of the different-sized PEG molecules on the properties of conjugated Gal3C to test their effects on solvent accessibility and conjugate thermal stabilization.[22] We used 2D IR spectroscopy to investigate how PEGylation altered the backbone of conjugated Gal3C and investigate the impact of PEGylation on protein−solvent interactions and solvent exposure. NMR spectroscopy provided complementary insights into the influence of conjugated PEG on the protein backbone at slower time scales and was also used to quantify the diffusion properties of PEGylated Gal3C. These measurements enabled us to correlate changes in solvation networks with the dumbbell and shroud models of protein-PEG interactions. MD simulations further complemented our experimental data by visualizing the conjugated polymer and providing a global characterization of solvation environments and backbone flexibility.[41−43] Together, these integrated approaches enabled us to correlate polymer length with changes in the solvation network of the conjugated protein and its stability, providing mechanistic insights into the intentional design of protein−polymer conjugates with predictable properties.

https://doi.org/10.1021/jacsau.5c01692
JACS Au 2026, 6, 1801−1811

RESULTS

Conjugation of Gal3C with PEG

To examine the impact of PEG on the conformational dynamics and solvent organization of conjugated Gal3C, we compared unconjugated Gal3C with two Gal3C conjugates, each linked to poly(ethylene glycol) (PEG) of molecular weight of either 550 Da or 5 kDa, referred to here as Gal3C-PEG 550 Da or Gal3C-PEG 5 kDa, respectively. Gal3C PEGylation was performed using maleimide-functionalized PEG, which reacted specifically with a single extrinsic cysteine at position 243 in Gal3C[T243C]. We refer to this modified protein as Gal3C throughout the text. Gal3C-PEG 5 kDa was prepared according to previously reported protocols,[23] while Gal3C-PEG 550 Da was prepared using a similar protocol, substituting maleimide-PEG 5 k with a functionalized maleimide-PEG starting material of 550 Da (Section S1). Previous studies demonstrated that the *N*-methylmaleimide linker used to covalently attach PEG to Gal3C had no impact on the thermal stability of the protein and resulted in only subtle changes to the protein surface limited to a local region near the conjugation site.[23]

Due to the inability to resolve unconjugated Gal3C and Gal3C-PEG 550 Da via gel filtration chromatography, PEGylation efficiency of Gal3C-PEG 550 Da was measured using fluorescence spectroscopy with the thiol-reactive fluorescent dye *N*-[4-(7-diethylamino-4-methyl-3-coumarinyl)-phenyl]maleimide (CPM). By measuring the fluorescence spectra of Gal3C-PEG 550 Da in the presence of CPM, we determined that >85% of Gal3C was successfully conjugated following the reaction protocol described in Section S1 (Figure S1). To test the activity of Gal3C-PEG 550 Da we recorded tryptophan fluorescence spectra to quantify the binding affinity of lactose to Gal3C-PEG 550 Da and compared this value to the binding affinity of lactose to Gal3C and Gal3C-PEG 5 kDa (Figure S2). The observed K_d values for lactose to Gal3C, Gal3C-PEG 550 Da and Gal3C-PEG 5 kDa were essentially identical, confirming that Gal3C-PEG 550 Da retained native activity (Figure S2).

To assess the impact of PEG 550 Da conjugation on the thermal stability of Gal3C, we recorded circular dichroism (CD) spectra from 200 to 280 nm (Figure S3). CD spectra of Gal3C-PEG 550 Da at 30 °C were consistent with a well-folded protein containing mostly β-sheet secondary structure and were at most only marginally different from CD spectra of Gal3C and Gal3C-PEG 5 kDa recorded at the same temperature (Figure S3). Temperature-dependent CD spectra recorded with Gal3C-PEG 550 Da showed a single cooperative unfolding transition with an apparent T_m of ∼58 °C with a λ_{min} of 225 nm. The thermal unfolding behavior of Gal3C-PEG 550 Da was highly similar to that of Gal3C but contrasted starkly to the thermal unfolding behavior of Gal3C-PEG 5 kDa. Consistent with earlier findings,[23] thermal unfolding of Gal3C-PEG 5 kDa showed two separate unfolding transitions and the formation of an intermediate conformation, as evidenced by a shift in λ_{min} from 225 to 215 nm (Figure S3). This stark contrast in the thermal unfolding behavior between Gal3C-PEG 550 Da and Gal3C-PEG 5 kDa motivated a deeper investigation into the molecular mechanisms underlying these distinct unfolding pathways.

"Shroud-like" Protein–Polymer Conformation is Observed for Gal3C PEGylated with PEG 5 kDa but Not with PEG 550 Da

The extent of interaction between the protein and polymer affects the diffusion behavior of the protein–polymer conjugate. For the dumbbell model, minimal interaction allows the protein and polymer to behave as independent molecules, and we would predict that the diffusion behavior of such a system would be nearly identical to the unconjugated protein. In contrast, for the shroud model, more extensive protein–polymer interactions would decrease the rate of diffusion of the system relative to the unconjugated protein. Thus, by measuring the diffusion properties of the conjugated protein, it is possible to distinguish between the two proposed models. NMR spectroscopy can be used to quantify the diffusion properties of conjugates by measuring the rotational correlation time (τ_c) of the conjugated protein. We determined τ_c values by measuring the ^{15}N longitudinal (T_1) and transverse (T_2) relaxation times of the backbone. This approach has been used to quantitatively determine rotational correlation times for globular proteins up to ∼25 kDa.[44,45] Previously, we determined the τ_c values for Gal3C and Gal3C–PEG 5 kDa (Section S3) and showed that PEGylation increased the rotational correlation time of Gal3C from 10.6 (±0.7) ns to 12.0 (±0.8) ns. This was consistent with observed increased line broadening in ^{15}N-edited ^{1}H NMR spectra of Gal3C–PEG 5 kDa and an increased transverse relaxation time. The increased τ_c value for Gal3C–PEG 5 kDa was interpreted as supporting a shroud-like conformation of the polymer within the protein–polymer conjugate. Here, we tested whether the shorter chain PEG in conjugated Gal3C-PEG 550 Da also formed a shroud-like conformation by measuring the τ_c value for Gal3C-PEG 550 Da. Unlike Gal3C–PEG 5 kDa, we determined a τ_c value for Gal3C-PEG 550 Da to be 10.6 (±1.0) ns, which is similar to the τ_c value measured for Gal3C and significantly shorter than the τ_c value measured for Gal3C–PEG 5 kDa (Figure 2 and Section S3). The similar τ_c values for Gal3C and Gal3C-PEG 550 Da are consistent with similar line widths observed in their respective ^{15}N-edited ^{1}H NMR spectra (Figure S4). Together, these data support a shroud-like model for Gal3C–PEG 5 kDa and a more dumbbell-like model for Gal3C-PEG 550 Da.

As shown in previous NMR studies of PEGylated proteins, 2D [^{15}N,^{1}H]-heteronuclear single quantum correlation (HSQC) spectra can reveal the impact of PEGylation on the protein backbone conformation and dynamics, as manifested by changes in chemical shifts or line broadening upon PEGylation. To observe the extent to which PEGylation with the shorter, 550 Da polymer impacted conjugated Gal3C structure and dynamics, we recorded 2D [^{15}N,^{1}H]-HSQC spectra of Gal3C–PEG 550 Da at 30 °C (Figure S4). [^{15}N,^{1}H]-HSQC spectra of Gal3C–PEG 550 Da were well dispersed, consistent with a well-folded protein as expected from the CD measurements. Comparison of the [^{15}N,^{1}H]-HSQC spectra of [u-^{15}N] Gal3C–PEG 550 Da with [u-^{15}N] Gal3C and [u-^{15}N] Gal3C–PEG 5 kDa showed that the spectra largely overlapped, indicating that conjugation with PEG 550 Da did not change the overall folding of Gal3C (Figure S4). We also compared these data with HSQC spectra of [u-^{15}N] Gal3C- PEG 550 Da to Gal3C conjugated with *N*-methylmaleimide without PEG, [u-^{15}N] Gal3C-NMM. These spectra were also largely overlapped. The high resolution and dispersion of the HSQC spectra facilitated a more detailed

https://doi.org/10.1021/jacsau.5c01692
JACS Au 2026, 6, 1801–1811

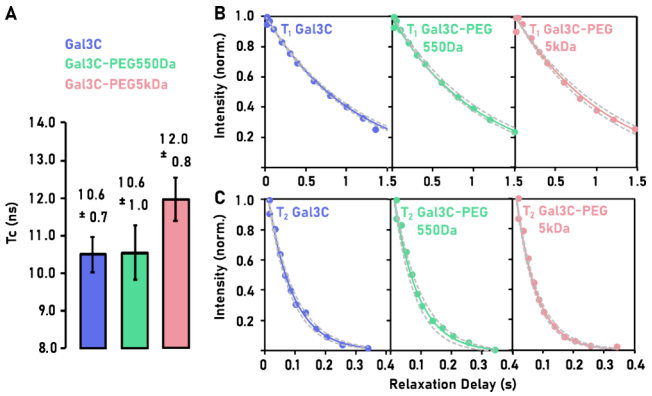

Figure 2. Rotational diffusion rates of Gal3C, Gal3C-PEG 5 kDa, and Gal3C-PEG 550 Da. (A) Rotational correlation times (τ_c) of Gal3C (blue), Gal3C-PEG 550 Da (green) and Gal3C-PEG 5 kDa (pink) at 30 °C determined from ^{15}N relaxation. (B) Global ^{15}N longitudinal relaxation times (T_1) of amide groups in the structured core of Gal3C, Gal3C-PEG 550 Da and Gal3C-PEG 5 kDa. (C) Global ^{15}N transverse relaxation times (T_2) of amide groups in the structured core of Gal3C, Gal3C-PEG 550 Da and Gal3C-PEG 5 kDa. Solid circles represent normalized integral values obtained for each relaxation delay, and the solid lines are the nonlinear regression used to quantify T_1 and T_2. Dotted lines indicate 95% confidence intervals from the regression procedure. The T_1 and T_2 values are computed and presented in Table S1.

comparison of the chemical shifts and line widths among [u-^{15}N] Gal3C, [u-^{15}N] Gal3C−PEG 550 Da and [u-^{15}N] Gal3C−PEG 5 kDa. By comparing chemical shift perturbations between Gal3C and Gal3C−PEG 550 Da, we observed that conjugation with PEG 550 Da resulted in minor perturbations, primarily localized to the conjugation site, indicating that conjugation with PEG 550 Da resulted in only minor perturbations to the Gal3C backbone (Figure 3). Except for one residue near position 220, we observed at most only minimal line broadening, typically less than 20 Hz, across all residues in spectra of Gal3C−PEG 550 Da.

In contrast to these observations, more pronounced differences were observed when comparing HSQC spectra of Gal3C and Gal3C−PEG 5 kDa. Conjugation of Gal3C with PEG 5 kDa resulted in larger chemical shift perturbations, particularly between residues 134−140, 193−200, 219, and 249. Additionally, Gal3C−PEG 5 kDa exhibited more extensive line broadening, with most residues showing increased line broadening of ≥20 Hz, and residues near the conjugation site showing greater line broadening of ≥40 Hz. Together, the HSQC data and rotational diffusion measurements for Gal3C−PEG 550 Da and Gal3C−PEG 5 kDa suggest that the longer PEG chain interacts more extensively with Gal3C, influencing both residue-level conformation and dynamics, as well as macromolecular diffusion properties. These findings support a model in which Gal3C−PEG 5 kDa adopts a shroud-like conformation, whereas Gal3C−PEG 550 Da assumes a more dumbbell-like structure.

2D IR Indicates that PEGylation Influences Protein Conformation and Its Local Environment on Ultrafast Time Scales

We investigated the impact of PEGylation on the conformation and environment around the Gal3C backbone on ultrafast time scales by recording 2D IR spectra of Gal3C, Gal3C−PEG 550 Da and Gal3C−PEG 5 kDa from 150 to 3000 fs. Examples of correlation maps are shown in Figure 4. The amide I band, corresponding to the backbone amide I stretching mode, provides insights into changes to the global protein structure and environment. Here we used amide I as a marker band to determine the impact of PEGylation in the Gal3. The 2D spectra of unconjugated Gal3C, Gal3C−PEG 550 Da and Gal3C−PEG 5 kDa show one pair of major peaks along the diagonal, where the red and blue colors represent positive or negative peaks, corresponding to transitions from ground to first excited, or first-to-second excited states, respectively.[22,46] In all spectra, an elongated peak shape across the amide I stretching region is observed with two main peak centers near 1630 and 1680 cm^{-1}, corresponding to the antiparallel and parallel β-sheet vibrations, respectively[22] (Figure 5). Notably, the positive peak elongation is more pronounced for Gal3C−PEG 550 Da compared to unconjugated Gal3C, and this elongation is further enhanced for Gal3C−PEG 5 kDa, this trend is observed over the waiting times. The peak elongation is assigned to the introduction of PEGylation and could be related to main factors: 1. the increase of structural heterogeneity and/or the solvent exposure, 2. energy transfer among the amide I modes. The pronounced elongation observed in the positive peak for Gal3C−PEG 5 kDa is an indication that the long PEG chain would induce more significant conformational disorder and/or solvent interaction compared to the small PEG chain. Additionally, at short waiting time (t_2) such as 150 fs (Figure 4, left), the peak is diagonally elongated, that can be interpretated as a strong correlation between excitation and detection frequencies. At longer t_2, the initial diagonal correlation diminishes as structural heterogeneity, solvent interactions, and vibrational energy transfer randomize frequencies (Figure 4, right, and Figures S5−S7).

Amide I absorption spectra report on backbone structure, thus we computed the pump slice amplitude (PSA) from the 2D IR spectra at 150 fs to extract features comparable to FTIR spectra. In brief, PSA analysis projects a 1D spectrum at each excitation frequency and computes the difference between the maxima and the minima of a series of pump−probe slices.[47] We selected a waiting time of 150 fs to avoid pulse-overlap artifacts while ensuring that peak shapes remained unaffected by energy dissipation, which occurs at longer waiting times. The PSAs of Gal3C and Gal3C−PEG 550 Da exhibit a maximum around 1630 cm^{-1} (Figure 5A). Relative to Gal3C and Gal3C−PEG 550 Da, the maximum of Gal3C−PEG 5 kDa shows a 5 cm^{-1} redshift, likely indicating an increase in antiparallel β-sheet structures or changes in the backbone dihedral angles that lower the vibrational frequency. Both Gal3C−PEG 550 Da and Gal3C−PEG 5 kDa exhibit broader lineshapes between 1650 and 1680 cm^{-1} compared to Gal3C, with the effect being more pronounced for Gal3C−PEG 5 kDa. These findings suggest that PEGylation, particularly with the long PEG chain (5 kDa), would increase the structural heterogeneity, likely due to increased flexibility and solvent exposure in β-turn/loop regions of the backbone.[48]

Conjugation with Longer PEG Likely Alters the Solvation Network at the Gal3C Surface

To clarify the influence of PEGylation on Gal3C, we analyzed the 2D IR line shape evolution for the three systems under investigation using center line slope (CLS) analysis (Figure 5B,C). The CLS is obtained by identifying the detection frequencies (vertical axis) with the ridge of maximum intensity along the excitation axis (horizontal axis) and then fitting a

https://doi.org/10.1021/jacsau.5c01692
JACS Au 2026, 6, 1801−1811

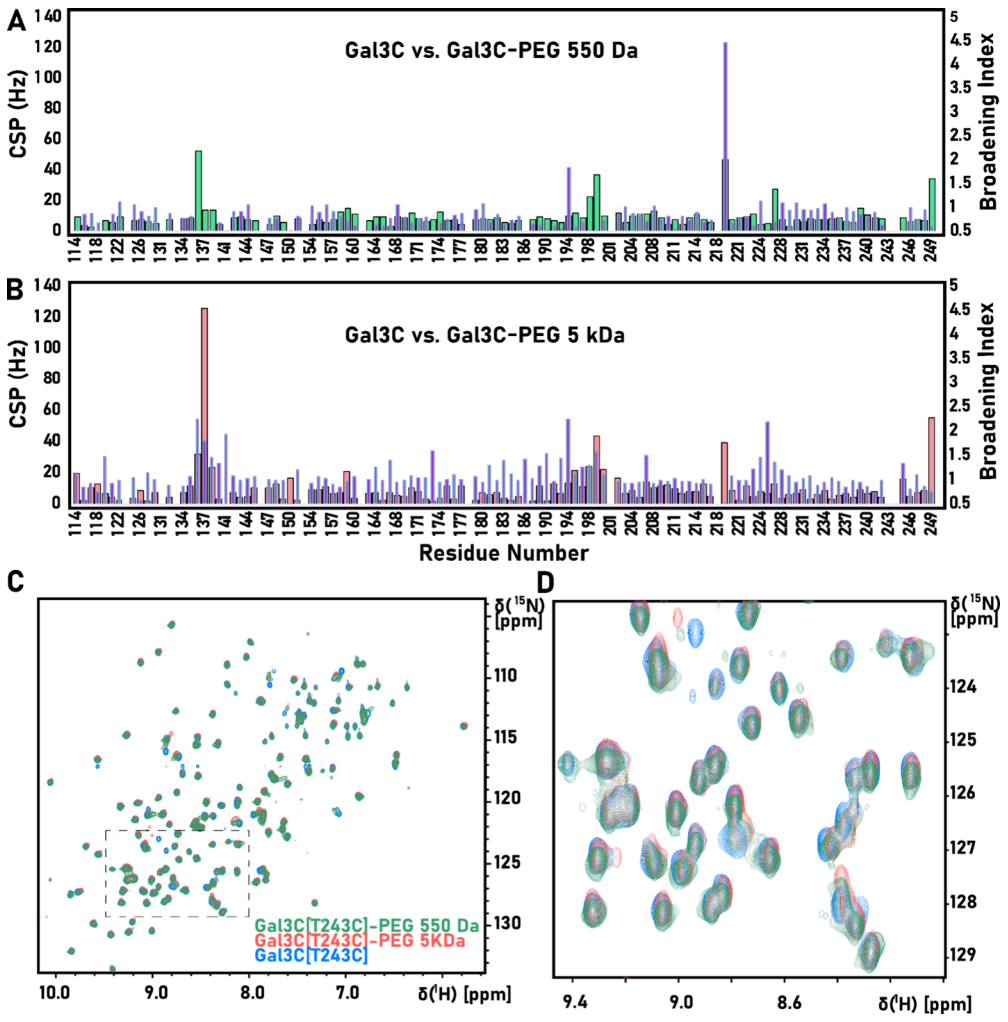

Figure 3. Histogram of the chemical shift perturbations (green and pink bars) and line broadening (purple bars) observed for (A) Gal3C relative to Gal3C−PEG 550 Da, (B) Gal3C relative to Gal3C−PEG 5 kDa as a function of the residue position. (C) Superposition of [^{15}N,^{1}H]-HSQC spectra of [u-^{15}N]-Gal3C (blue), [u-^{15}N]-Gal3C−PEG 5 kDa (red) and [u-^{15}N]-Gal3C−PEG 550 Da (green) measured at 30 °C. (D) Expanded view from the dashed box shown in panel (C).

linear slope through these points (Section S4).[49,50] The CLS decays fit well to a monoexponential function (Figure 5C), serving as an experimental measure of the frequency−frequency correlation function (FFCF). More specifically, FFCF reflects the decorrelation between excitation and detection frequencies with waiting time, capturing the environmental fluctuations along the backbone.[49,51] The CLS analyses indicate similar decay time constants for Gal3C and Gal3C−PEG 550 Da, but Gal3C−PEG 5 kDa shows a decay almost twice as slow as that of the other two systems. These results suggest that the long PEG chain significantly slows the local dynamics, while the short PEG chain has minor influence on dynamics.

Picosecond frequency fluctuations extracted from 2D IR spectra provide insight into the hydrogen-bond dynamics between amide groups and surrounding water molecules.[52−54] The origins of the effects observed on the dynamics of the PEGylated proteins could be due to multiple reasons, including more restricted fluctuations of the residues upon polymer contact, backbone dehydration, and less mobile water around the backbone. The distinct outcomes observed for the short and long PEG chains suggest that they may adopt different configurational models. The longer PEG chain could plausibly assume a "shroud-like" arrangement, in which contacts between the polymer and certain protein residues influence local hydrogen-bond rearrangements. In such a scenario, the reorientation of water molecules required for hydrogen-bond exchange might be partially hindered by the presence of the PEG chain. This effect could, in turn, extend the lifetime of C═O-water hydrogen bonds and contribute to slower reorganization within the solvation shell. That said, based on the experimental data alone, it remains difficult to clearly identify or visualize the dominant factor responsible for the slower dynamics observed in Gal3C−PEG 5 kDa. Therefore, we complemented the experiments with molecular dynamics (MD) simulations to gain a deeper understanding of the system.

MD Simulations Elucidate and Visualize the Structure and Environment of Gal3C and PEGylated Gal3C

To evaluate the proposed shroud model in the context of changes to the local environment along the protein backbone, MD simulations were performed for three systems: Gal3C, Gal3C−PEG 600 Da and Gal3C−PEG 5 kDa. For the MD simulations, we used PEG600, which contains 13 repeating units, whereas the PEG550 used in the experiments has an average of 12.5 repeating units. The 600 Da chain length was

https://doi.org/10.1021/jacsau.5c01692
JACS Au 2026, 6, 1801−1811

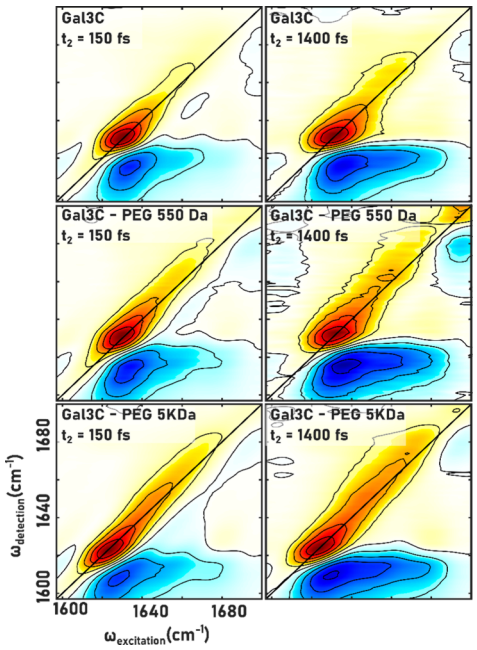

Figure 4. 2D IR spectra of Gal3C, Gal3C−PEG 550 Da and Gal3C−PEG 5 kDa at two selected waiting times, t_2 = 150 and t_2 = 1400 fs, as indicated in the panels.

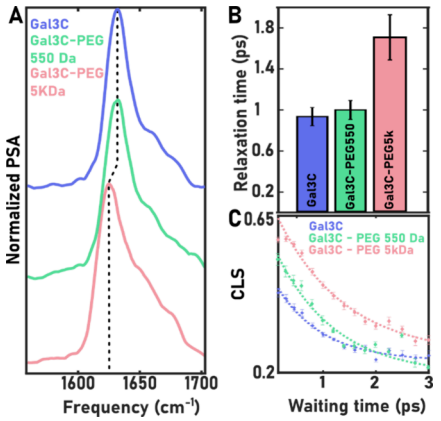

Figure 5. 2D IR spectral analysis for protein structure and dynamics. (A) PSA at waiting time of 150 fs for Gal3C, Gal3C−PEG 550 Da and Gal3C−PEG 5 kDa. (B) Relaxation time constants extracted from the exponential fits of CLS analysis. Fitting parameters were evaluated through a bootstrapping technique to estimate the standard error of the fits. The error bars are the standard errors of the time constants estimated from the standard deviation of the fitted curves. (C) CLS decay as a function of the waiting time. The CLS curves fit to a monoexponential function (dashed lines). See Section S4 for details of CLS analysis.

chosen because each monomer contributes a fixed molecular weight, allowing us to match the experimental system as closely as possible. Importantly, no significant differences in the computational results are expected between PEG550 and PEG600. Further details of the simulation setup and parameters are provided in Section S5. For PEG conjugation, a covalent bond was introduced between the first carbon atom of the PEG chain and the sulfur atom of cysteine residue 243 of Gal3C (see Section S5). This approach was used instead of the experimentally employed maleimide linkage, because corresponding parameters are not currently available in the CHARMM force field for such a linkage. We expect that this substitution would not affect the simulation results, as previous experimental characterization indicated that the maleimide linkage has minimal or no impact on the biophysical or functional properties of the conjugated protein (see above and previously published studies).[23,55]

The root mean squared displacement (RMSD) of protein residues was computed to assess the equilibrium of the simulated proteins, which shows that all systems reached a stable state after 100 ns trajectory (Figure S8). Accordingly, all structural analyses were conducted using the trajectory after 100 ns. To visualize the effects of the conjugated short and long PEG chains, the modeled structures of PEGylated Gal3C are shown in Figure 6A, with additional orientations shown in Figure S9. For Gal3C conjugated with the short PEG chain, only a small region near the conjugation site at residue 243 is covered, resembling the protein wearing a "hat". In contrast, the flexible and extended long PEG (5 kDa) chain covers a substantial portion of the protein surface, particularly the back and sides, giving the appearance of a "backpack". This larger PEG chain thus produced more pronounced "shrouding" effects, with potential global impacts on the protein backbone such as increased dehydration, protection, and shielding from the surrounding environment.

To gain further insights into the interactions between the protein and PEG chains, the minimum distance between the PEG chain and each protein residue was computed. A cutoff distance of 0.35 nm was used to define direct contacts. A residue was considered in contact with PEG when the interatomic distance fell below this threshold. The contact probability for each residue was then calculated as the fraction of simulation frames in which such contact occurred over the total number of frames (Figure 6B). This analysis revealed that atoms in the long PEG chain engage in more sustained interactions with protein residues compared to those with the short PEG chain. These differences are evident for the residues between 131 and 141, 191−202, 214−216 and 241−250 (Figure 6B), this is in alignment with the chemical shift perturbations measured by NMR, where the strongest perturbations were expected around residues 134−140, 193−200, 219, and 249 (Figure 3). In addition, the long PEG chain tends to remain in contact with the protein more frequently and for longer periods compared to the short PEG chain (Figure S10). Notably, the contacts between the long PEG chain and protein are especially prolonged for residues 131−141 and 191−202 (Figure S10).

To examine the effects of PEGylation on protein dynamics, the root mean squared fluctuations (RMSF) of the protein residues was computed and compared between unmodified Gal3C and the PEGylated (Figure S11). In both Gal3C−PEG 600 Da and Gal3C−PEG 5 kDa, most residues exhibited reduced fluctuations, indicating that PEGylation imposed a global conformational constraint across the entire protein. Visualization of these effects using color-coded models (Figure S12) showed that the front (sugar-binding surface) and back of the protein are minimally affected, whereas portions of the side β-sheets and several random coils exhibit restricted mobility in the presence of PEG. Although PEG 5 kDa shows more pronounced restriction effects than PEG 600 Da, the affected residues are largely overlapping between the two structures. Therefore, the difference between short and long PEG in the results of NMR and 2D IR is unlikely due to the mobility restrictions imposed by PEGylation.

https://doi.org/10.1021/jacsau.5c01692
JACS Au 2026, 6, 1801−1811

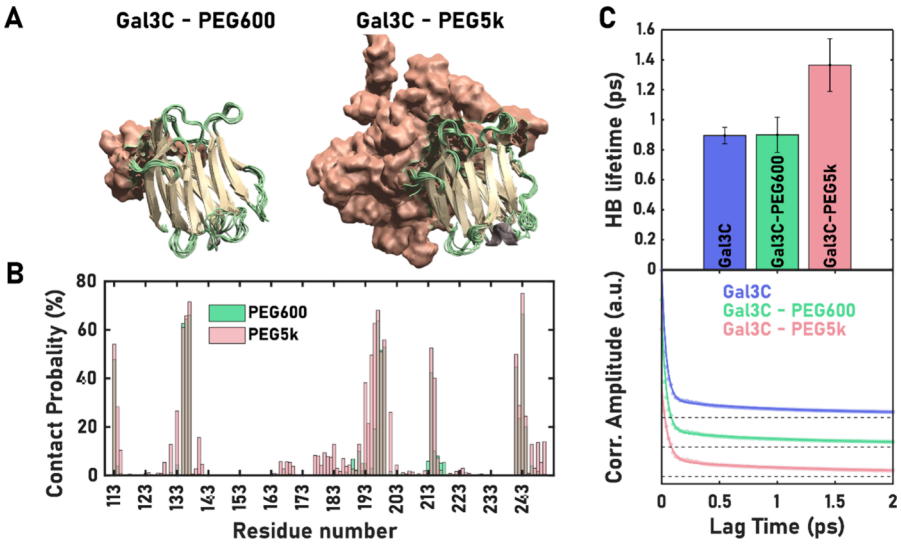

Figure 6. Summary of important results from MD analysis. (A) Snapshots from the MD trajectories every 10 ns for both Gal3C−PEG 600 Da and Gal3C−PEG 5 kDa were superimposed. PEG chains are shown in the pink surface representation, while the yellow, purple and green colors represent the β-sheet, random coil/turn and α-helical secondary structure of Gal3C, respectively (ribbon representation). (B) Contact probability (%) between PEG and each Gal3C residue was computed with a cutoff distance of 0.35 nm. (C) HB lifetime analysis and associated fittings for the correlation functions of hydrogen-bond number. The error bars for the fitting parameters were calculated as the standard deviation of the parameters obtained from 10 independent production runs. Details of the MD analysis are described in Section S5.

Conjugation with Longer PEG Does Not Dehydrate the Protein Surface but Alters Solvent Dynamics and the Lifetimes of Protein−Solvent Interactions

To test the impact of PEGylation on solvent exposure of the Gal3C backbone, we computed the solvent accessible surface area (SASA) for the three systems (Figure S13). The SASA values were calculated for the entire protein (backbone and side chains), although backbone exposure is emphasized here to enable direct comparison with 2D IR measurements. Overall, the effects of PEGylation on protein hydration are quite diverse, depending on the position of the residues. In agreement with NMR data,[23] the protein sugar-binding pocket surface was minimally affected by the PEG chain. Though the changes in residue hydration are more prominent in PEG 5 kDa, the altered residues largely overlap between the two PEGylated proteins. We quantified the total number of hydrogen bonds between water and the protein backbone. Interestingly, the hydrogen-bond number for Gal3C, Gal3C−PEG 600 Da and Gal3C−PEG 5 kDa were all similar at 77.1, 76.5, and 76.4, respectively. This indicates that conjugation with a longer PEG does not dehydrate the protein surface and supports the notion that the differences observed in the behavior of Gal3C−PEG 5 kDa, compared to Gal3C-PEG 600 Da and unconjugated Gal3C in 2D IR and NMR experiments, are not attributable to replacement of water molecules.[39,40]

The hydrogen-bond lifetime, averaged among all the hydrogen bonds formed between protein amide groups and the nearby molecules (Figure 6C), quantifies effects of PEGylation on hydrogen-bond dynamics around the protein backbone. The hydrogen-bond autocorrelation exhibits a decay constant on the picosecond scale, which is associated with the process of hydrogen bond formation and dissociation.[56,57] Gal3C conjugated with the short PEG chain shows no discernible change in the lifetime, while the long PEG chain leads to a ∼50% slowdown, as compared to unconjugated Gal3C (Table S3). The time scales of computed hydrogen-bond lifetimes are comparable to the relaxation time extracted from CLS analysis of 2D IR, where the slowdown in hydrogen-bond lifetime qualitatively agrees with the slower dynamics observed in the 2D IR experiments for Gal3C−PEG 5 kDa (Figure 5B).

In the dynamics analysis of the 2D IR data, the frequency fluctuations in the amide I vibrational range can be interpreted as related to the rapid hydrogen-bond fluctuations between protein amide groups and nearby water molecules.[52−54] To evaluate this interpretation with the MD simulations, we conducted a population analysis of hydrogen bonds (Figure S14), finding that those formed between amide groups and water (intermolecular) account for approximately 50% of the total, whereas amide−amide hydrogen bonds represent about 45% (intramolecular). Based on that amide−water interactions would be slightly more prevalent than amide−amide interactions. The fluctuations in hydrogen-bond number further distinguish these two populations, the standard deviation in the number of amide−water hydrogen bonds is higher than that of amide−amide bonds, indicating greater dynamic variability. This trend is consistent with the larger amplitude observed in the autocorrelation function of the amide−water hydrogen-bond number.

In terms of hydrogen-bond lifetime (Figures S15 and S16 and Tables S4 and S5), amide−amide hydrogen bonds persist longer than those formed with water. Additionally, the lifetime of intermolecular hydrogen bonds is similar for Gal3C and Gal3C−PEG 600 but becomes noticeably longer for Gal3C−PEG 5k, in line with the slowdown in solvent dynamics inferred from the spectroscopic data (Figure 5B). The lifetime of intramolecular hydrogen bonds, however, shows a different trend, where it slows down from Gal3C, to Gal3C−PEG 600 and then to Gal3C−PEG 5k. When these observations are considered together with the 2D IR measurements, we can provide a more coherent picture of the system. Our MD results suggest that both intra- and intermolecular hydrogen bonds contribute to the slower dynamics observed in Gal3C−PEG5 kDa. However, the contribution to the FFCF appears to be

https://doi.org/10.1021/jacsau.5c01692
JACS Au 2026, 6, 1801−1811

higher for intermolecular hydrogen bonds, as intramolecular hydrogen bonds fluctuate with relatively low amplitude. Putting this together with the experimental time scale (0−3 ps), we can suggest that the lifetimes of amide−water hydrogen bonds are expected to exert a stronger influence on the measured dynamics than amide−amide interactions. Thus, the MD analysis of intra- and intermolecular hydrogen bonding supports the interpretation that water dynamics are likely the primary drivers of the effects observed by 2D IR.

DISCUSSION

The 2D IR measurements and MD simulations support a model in which PEGylation stabilizes Gal3C by reorganizing solvent dynamics within the surrounding protein solvent shell without any measurable changes to the protein secondary structure. Neither 2D IR nor MD simulations detected evidence for PEGylation-driven desolvation of the protein surface or significant differences in the SASA among Gal3C, Gal3C−PEG 550 and Gal3C−PEG 5k. While the SASA was investigated in the present study at picosecond to nanosecond time scales, our findings align with earlier observations from NMR spectroscopic studies that showed PEGylation did not alter the SASA of Gal3C over longer time scales.[23] Instead, we observed that PEGylation slows solvent dynamics surrounding the surface of Gal3C, with the magnitude of this effect correlating with the length of the conjugated polymer. PEGylation-driven slowing of solvent dynamics correlated with the formation of a shroud-like protein-PEG conformation and with the increased thermal stability and redirection of the Gal3C unfolding pathway. These observations are of interest in the context of related studies of protein−polymer conjugates and investigations into mechanisms of stabilization of proteins via PEGylation.

Our investigation focused on polymer length within conjugates containing a single site available for chemical modification. Overall, the present results are consistent with prior experimental and computational studies indicating that a minimum polymer length is required to increase the melting temperature of the conjugated protein, a trend that also extends to nonlinear or branched polymers. In contrast, earlier studies employing multiple PEGylation sites have revealed different trends. For chymotrypsin PEGylated simultaneously at multiple lysines, once a sufficient number of residues were modified, thermal stability was observed to depend more strongly on the degree of modification than on polymer length.[58] Together, these observations support a "coverage" model in which a minimum extent of protein−polymer interaction is required to produce significant stabilization. For single-site conjugates, this threshold is achieved by increasing PEG molecular weight, whereas for multisite conjugates it is reached by PEGylating a sufficient number of residues.

Specific properties of proteins may also influence the characteristics of PEGylated conjugates. A comparison of Gal3C with chymotrypsin from prior studies indicates that the two proteins have broadly similar distributions of hydrophobic and hydrophilic surface regions. However, the corresponding PEGylated systems differ in both conjugation chemistry and extent of modification.[58] Gal3C is modified at a single cysteine, whereas chymotrypsin was PEGylated at multiple lysines, with up to 9 of its 14 lysines reported to be modified.[58] The specific lysines involved were not identified, limiting more detailed surface-level comparisons between the two conjugates. These differences may, at least in part, underlie the contrasting conclusions regarding solvent-accessible surface area, namely a reported decrease for PEGylated chymotrypsin versus the residue-dependent SASA changes observed here for PEGylated Gal3C, which do not show a clear global trend (Figure S13).[58] Comparisons with human insulin further highlight the importance of relative protein size. In simulations, PEG200 effectively enveloped the much smaller insulin,[43] whereas even the largest PEG used here did not fully cover Gal3C. This distinction may have contributed to the differing conclusions that PEGylation reduces the SASA of insulin, particularly for the largest PEG studied.

It is also of interest to consider whether the conjugation site may influence the properties of PEGylated proteins. Prior studies of Pin1 indicated that local sequence context can influence stabilization.[32] Conjugation sites adjacent to residues containing hydroxyl groups tended to lead to PEGylated proteins with increased thermal stability. However, computational analyses suggested these effects arose through indirect interactions among PEG, the protein, and surrounding solvent rather than directly through protein-PEG interactions.[32] Prior computational work on bovine serum albumin (BSA) proposed that interactions between lysine side chains and PEG were a major contributing factor to PEG localization and conjugate properties.[41] However, our earlier experimental biophysical studies showed that while lysines influenced the localization of PEG, lysine−PEG interactions alone did not account for the enhanced stability of PEGylated Gal3C.[23] Collectively, these findings support a more nuanced mechanism in which multiple types of protein−polymer and protein−solvent interactions determine the properties of PEGylated protein conjugates.

CONCLUSIONS

A key strength of 2D IR spectroscopy is its ability to directly probe molecular processes on picosecond to nanosecond time scales, which we exploited here to examine both the protein and its surrounding solvent in a PEGylated conjugate. By integrating 2D IR measurements with site-specific structural information from NMR and with diffusion data for PEGylated Gal3C, we link features of protein solvation, which occur on relatively faster molecular time scales, to conformational and diffusion processes, which occur on relatively slower molecular time scales. Although extending this approach to a broad set of PEGylated proteins, particularly those with distinct secondary structures, could offer additional insights, achieving comparable depth across many systems would be resource-intensive and arguably not practical. In this context, the combination of the present experimental results with computational simulations provides a benchmark for scaling studies of protein−polymer conjugates in a more efficient and generalizable manner via entirely computational approaches in future studies.

Given the multifaceted nature of protein−polymer interactions, a reasonable hypothesis is that multiple mechanisms likely exist that rationalize protein stabilization via PEGylation. The impact of PEG on the stability of conjugates will likely depend on protein-specific surface properties and intrinsic dynamics of both the protein and conjugated polymer. Moreover, for systems where the PEG chain does not fully cover the surface of the protein, the location of the conjugation site is likely to influence polymer conformational behavior and its impact on local hydration and dynamics. Site-directed

https://doi.org/10.1021/jacsau.5c01692
JACS Au 2026, 6, 1801−1811

PEGylation, as used here, provides a controlled framework to dissect these effects, and the agreement between experiment and simulation suggests that molecular modeling can be a valuable tool for predicting how protein type and attachment geometry shape PEG-protein interactions.

■ ASSOCIATED CONTENT

Data Availability Statement

The data supporting this article have been included as part of the Supporting Information.

Supporting Information

The Supporting Information is available free of charge at https://pubs.acs.org/doi/10.1021/jacsau.5c01692.

Details of protocols followed for protein expression and sample preparation, details for experimental methods for sample characterization, including circular dichroism, and details on methods and analysis of NMR data and additional NMR spectra. Experimental details of the 2D IR measurements, additional measured 2D IR spectra, IR data analyses and details of the MD simulations, and analysis of the trajectories (PDF)

■ AUTHOR INFORMATION

Corresponding Authors

Matthew T. Eddy − *Department of Chemistry, University of Florida, Gainesville, Florida 32611, United States;* orcid.org/0000-0002-3349-6212; Email: matthew.eddy@ufl.edu

Carlos R. Baiz − *Department of Chemistry, University of Texas at Austin, Austin, Texas 78712, United States;* orcid.org/0000-0003-0699-8468; Email: cbaiz@cm.utexas.edu

Authors

Raiza Maia − *Department of Chemistry, University of Texas at Austin, Austin, Texas 78712, United States*

Xiaobing Chen − *Department of Chemistry, University of Texas at Austin, Austin, Texas 78712, United States;* orcid.org/0000-0002-6107-1713

Emma Mulry − *Department of Chemistry, University of Florida, Gainesville, Florida 32611, United States*

Complete contact information is available at: https://pubs.acs.org/10.1021/jacsau.5c01692

Author Contributions

†R.M. and X.C. contributed equally.

Notes

The authors declare no competing financial interest.

■ ACKNOWLEDGMENTS

This work was supported by the Welch Foundation (F-1891) and the National Institutes of Health (R35GM133359). Simulations were run on the Lonestar6 cluster at the Texas Advanced Computing Center (TACC). M.T.E. and E.M. were supported by an NSF CAREER award 2339330 through the Division of Materials Research. A portion of this work was supported by the McKnight Brain Institute at the National High Magnetic Field Laboratory's AMRIS Facility, which is funded by the National Science Foundation Cooperative Agreement No. DMR-1644779.

■ REFERENCES

(1) Pham, J. V.; Yilma, M. A.; Feliz, A.; Majid, M. T.; Maffetone, N.; Walker, J. R.; Kim, E.; Cho, H. J.; Reynolds, J. M.; Song, M. C.; Park, S. R.; Yoon, Y. J. A Review of the Microbial Production of Bioactive Natural Products and Biologics. *Front. Microbiol.* **2019**, *10*, 1404.

(2) Anselmo, A. C.; Gokarn, Y.; Mitragotri, S. Non-Invasive Delivery Strategies for Biologics. *Nat. Rev. Drug Discovery* **2019**, *18* (1), 19−40.

(3) Scott, E. C.; Baines, A. C.; Gong, Y.; Moore, R.; Pamuk, G. E.; Saber, H.; Subedee, A.; Thompson, M. D.; Xiao, W.; Pazdur, R.; Rao, V. A.; Schneider, J.; Beaver, J. A. Trends in the Approval of Cancer Therapies by the FDA in the Twenty-First Century. *Nat. Rev. Drug Discovery* **2023**, *22* (8), 625.

(4) Pasut, G.; Veronese, F. M. State of the Art in PEGylation: The Great Versatility Achieved after Forty Years of Research. *J. Controlled Release* **2012**, *161* (2), 461−472.

(5) Grace, M. J.; Lee, S.; Bradshaw, S.; Chapman, J.; Spond, J.; Cox, S.; DeLorenzo, M.; Brassard, D.; Wylie, D.; Cannon-Carlson, S.; Cullen, C.; Indelicato, S.; Voloch, M.; Bordens, R. Site of Pegylation and Polyethylene Glycol Molecule Size Attenuate Interferon-α Antiviral and Antiproliferative Activities through the JAK/STAT Signaling Pathway. *J. Biol. Chem.* **2005**, *280* (8), 6327−6336.

(6) Harris, J. M.; Chess, R. B. Effect of Pegylation on Pharmaceuticals. *Nat. Rev. Drug Discovery* **2003**, *2* (3), 214−221.

(7) Krall, N.; Da Cruz, F. P.; Boutureira, O.; Bernardes, G. J. L. Site-Selective Protein-Modification Chemistry for Basic Biology and Drug Development. *Nat. Chem.* **2016**, *8* (2), 103−113.

(8) Shaunak, S.; Godwin, A.; Choi, J. W.; Balan, S.; Pedone, E.; Vijayarangam, D.; Heidelberger, S.; Teo, I.; Zloh, M.; Brocchini, S. Site-Specific PEGylation of Native Disulfide Bonds in Therapeutic Proteins. *Nat. Chem. Biol.* **2006**, *2* (6), 312−313.

(9) Gupta, S. K.; Pittenger, A. L.; Swan, S. K.; Marbury, T. C.; Tobillo, E.; Batra, V.; Sack, M.; Glue, P.; Jacobs, S.; Affrime, M. Single-Dose Pharmacokinetics and Safety of Pegylated Interferon-α2b in Patients with Chronic Renal Dysfunction. *Journal of Clinical Pharmacology* **2002**, *42* (10), 1109−1115.

(10) Zhang, B.; Sun, J.; Wang, Y.; Ji, D.; Yuan, Y.; Li, S.; Sun, Y.; Hou, Y.; Li, P.; Zhao, L.; Yu, F.; Ma, W.; Cheng, B.; Wu, L.; Hu, J.; Wang, M.; Song, W.; Li, X.; Li, H.; Fei, Y.; Chen, H.; Zhang, L.; Tsokos, G. C.; Zhou, D.; Zhang, X. Site-Specific PEGylation of Interleukin-2 Enhances Immunosuppression via the Sustained Activation of Regulatory T Cells. *Nat. Biomed. Eng.* **2021**, *5* (11), 1288−1305.

(11) Grigoletto, A.; Mero, A.; Zanusso, I.; Schiavon, O.; Pasut, G. Chemical and Enzymatic Site Specific PEGylation of HGH: The Stability and in Vivo Activity of PEG-N-Terminal-HGH and PEG-Gln141-HGH Conjugates. *Macromol. Biosci.* **2016**, *16* (1), 50−56.

(12) Zaghmi, A.; Mendez-Villuendas, E.; Greschner, A. A.; Liu, J. Y.; de Haan, H. W.; Gauthier, M. A. Mechanisms of Activity Loss for a Multi-PEGylated Protein by Experiment and Simulation. *Mater. Today Chem.* **2019**, *12*, 121−131.

(13) Baker, S. L.; Munasinghe, A.; Murata, H.; Lin, P.; Matyjaszewski, K.; Colina, C. M.; Russell, A. J. Intramolecular Interactions of Conjugated Polymers Mimic Molecular Chaperones to Stabilize Protein-Polymer Conjugates. *Biomacromolecules* **2018**, *19* (9), 3798−3813.

(14) Chang, P. K.; Prestidge, C. A.; Barnes, T. J.; Bremmell, K. E. Impact of PEGylation and Non-Ionic Surfactants on the Physical Stability of the Therapeutic Protein Filgrastim (G-CSF). *RSC Adv.* **2016**, *6* (82), 78970−78978.

(15) Hauptstein, N.; Pouyan, P.; Kehrein, J.; Dirauf, M.; Driessen, M. D.; Raschig, M.; Licha, K.; Gottschaldt, M.; Schubert, U. S.; Haag, R.; Meinel, L.; Sotriffer, C.; Lühmann, T. Molecular Insights into Site-Specific Interferon-A2a Bioconjugates Originated from PEG, LPG, and PEtOx. *Biomacromolecules* **2021**, *22* (11), 4521−4534.

(16) Cattani, G.; Vogeley, L.; Crowley, P. B. Structure of a PEGylated Protein Reveals a Highly Porous Double-Helical Assembly. *Nat. Chem.* **2015**, *7* (10), 823.

(17) Cerofolini, L.; Giuntini, S.; Carlon, A.; Ravera, E.; Calderone, V.; Fragai, M.; Parigi, G.; Luchinat, C. Characterization of PEGylated

Asparaginase: New Opportunities from NMR Analysis of Large PEGylated Therapeutics. *Chem. - Eur. J.* **2019**, *25* (8), 1984−1991.
(18) Le Cœur, C.; Combet, S.; Carrot, G.; Busch, P.; Teixeira, J.; Longeville, S. Conformation of the Poly(Ethylene Glycol) Chains in DiPEGylated Hemoglobin Specifically Probed by SANS: Correlation with PEG Length and in Vivo Efficiency. *Langmuir* **2015**, *31* (30), 8402−8410.
(19) Pai, S. S.; Hammouda, B.; Hong, K.; Pozzo, D. C.; Przybycien, T. M.; Tilton, R. D. The Conformation of the Poly(Ethylene Glycol) Chain in Mono-PEGylated Lysozyme and Mono-PEGylated Human Growth Hormone. *Bioconjugate Chem.* **2011**, *22* (11), 2317−2323.
(20) He, L.; Wang, H.; Garamus, V. M.; Hanley, T.; Lensch, M.; Gabius, H. J.; Fee, C. J.; Middelberg, A. Analysis of MonoPEGylated Human Galectin-2 by Small-Angle X-Ray and Neutron Scattering: Concentration Dependence of PEG Conformation in the Conjugate. *Biomacromolecules* **2010**, *11* (12), 3504−3510.
(21) Shu, J. Y.; Lund, R.; Xu, T. Solution Structural Characterization of Coiled-Coil Peptide-Polymer Side-Conjugates. *Biomacromolecules* **2012**, *13* (6), 1945−1955.
(22) Baiz, C. R.; Peng, C. S.; Reppert, M. E.; Jones, K. C.; Tokmakoff, A. Coherent Two-Dimensional Infrared Spectroscopy: Quantitative Analysis of Protein Secondary Structure in Solution. *Analyst* **2012**, *137* (8), 1793.
(23) Pritzlaff, A.; Ferré, G.; Mulry, E.; Lin, L.; Gopal Pour, N.; Savin, D. A.; Harris, M. E.; Eddy, M. T. Atomic-Scale View of Protein-PEG Interactions That Redirect the Thermal Unfolding Pathway of PEGylated Human Galectin-3. *Angew. Chem., Int. Ed.* **2022**, *61* (40), No. e202203784.
(24) Cheung, M. S.; García, A. E.; Onuchic, J. N. Protein Folding Mediated by Solvation: Water Expulsion and Formation of the Hydrophobic Core Occur after the Structural Collapse. *Proc. Natl. Acad. Sci. U. S. A.* **2002**, *99* (2), 685.
(25) Eisenberg, D.; Mclachlan, A. D. Solvation Energy in Protein Folding and Binding. *Nature* **1986**, *319* (6050), 199.
(26) Roder, H.; Colón, W. Kinetic Role of Early Intermediates in Protein Folding. *Curr. Opin. Struct. Biol.* **1997**, *7* (1), 15.
(27) Rhee, Y. M.; Sorin, E. J.; Jayachandran, G.; Lindahl, E.; Pande, V. S. Simulations of the Role of Water in the Protein-Folding Mechanism. *Proc. Natl. Acad. Sci. U. S. A.* **2004**, *101* (17), 6456.
(28) Fernández-Escamilla, A. M.; Cheung, M. S.; Vega, M. C.; Wilmanns, M.; Onuchic, J. N.; Serrano, L. Solvation in Protein Folding Analysis: Combination of Theoretical and Experimental Approaches. *Proc. Natl. Acad. Sci. U. S. A.* **2004**, *101* (9), 2834.
(29) Lawrence, P. B.; Price, J. L. How PEGylation Influences Protein Conformational Stability. *Curr. Opin. Chem. Biol.* **2016**, *34*, 88.
(30) Hamed, E.; Xu, T.; Keten, S. Poly(Ethylene Glycol) Conjugation Stabilizes the Secondary Structure of α-Helices by Reducing Peptide Solvent Accessible Surface Area. *Biomacromolecules* **2013**, *14* (11), 4053.
(31) Meng, W.; Guo, X.; Qin, M.; Pan, H.; Cao, Y.; Wang, W. Mechanistic Insights into the Stabilization of SrcSH3 by PEGylation. *Langmuir* **2012**, *28* (46), 16133.
(32) Lawrence, P. B.; Gavrilov, Y.; Matthews, S. S.; Langlois, M. I.; Shental-Bechor, D.; Greenblatt, H. M.; Pandey, B. K.; Smith, M. S.; Paxman, R.; Torgerson, C. D.; Merrell, J. P.; Ritz, C. C.; Prigozhin, M. B.; Levy, Y.; Price, J. L. Criteria for Selecting PEGylation Sites on Proteins for Higher Thermodynamic and Proteolytic Stability. *J. Am. Chem. Soc.* **2014**, *136* (50), 17547.
(33) Ferebee, R.; Hakem, I. F.; Koch, A.; Chen, M.; Wu, Y.; Loh, D.; Wilson, D. C.; Poole, J. L.; Walker, J. P.; Fytas, G.; Bockstaller, M. R. Light Scattering Analysis of Mono- and Multi-PEGylated Bovine Serum Albumin in Solution: Role of Composition on Structure and Interactions. *J. Phys. Chem. B* **2016**, *120* (20), 4591−4599.
(34) Dhalluin, C.; Ross, A.; Leuthold, L.-A.; Foser, S.; Gsell, B.; Mü, F.; Senn, H.; Hoffmann-La, F. Structural and Biophysical Characterization of the 40 KDa PEG-Interferon-α2a and Its Individual Positional Isomers. *Bioconjugate Chem.* **2005**, *16*, 504.
(35) Farhadi, S. A.; Bracho-Sanchez, E.; Fettis, M. M.; Seroski, D. T.; Freeman, S. L.; Restuccia, A.; Keselowsky, B. G.; Hudalla, G. A. Locally Anchoring Enzymes to Tissues via Extracellular Glycan Recognition. *Nat. Commun.* **2018**, *9* (1), 4943.
(36) John, C. M.; Leffler, H.; Kahl-Knutsson, B.; Svensson, I.; Jarvis, G. A. Truncated Galectin-3 Inhibits Tumor Growth and Metastasis in Orthotopic Nude Mouse Model of Human Breast Cancer. *Clin. Cancer Res.* **2003**, *9* (6), 2374.
(37) Mirandola, L.; Yu, Y.; Chui, K.; Jenkins, M. R.; Cobos, E.; John, C. M.; Chiriva-Internati, M. Galectin-3C Inhibits Tumor Growth and Increases the Anticancer Activity of Bortezomib in a Murine Model of Human Multiple Myeloma. *PLoS One* **2011**, *6* (7), No. e21811.
(38) Orengo, C. A.; Michie, A. D.; Jones, S.; Jones, D. T.; Swindells, M. B.; Thornton, J. M. CATH - A Hierarchic Classification of Protein Domain Structures. *Structure* **1997**, *5* (8), 1093.
(39) Fox, N. K.; Brenner, S. E.; Chandonia, J. M. SCOPe: Structural Classification of Proteins - Extended, Integrating SCOP and ASTRAL Data and Classification of New Structures. *Nucleic Acids Res.* **2014**, *42* (D1), D304.
(40) Sillitoe, I.; Bordin, N.; Dawson, N.; Waman, V. P.; Ashford, P.; Scholes, H. M.; Pang, C. S. M.; Woodridge, L.; Rauer, C.; Sen, N.; Abbasian, M.; Le Cornu, S.; Lam, S. D.; Berka, K.; Varekova, I. H.; Svobodova, R.; Lees, J.; Orengo, C. A. CATH: Increased Structural Coverage of Functional Space. *Nucleic Acids Res.* **2021**, *49* (D1), D266.
(41) Munasinghe, A.; Mathavan, A.; Mathavan, A.; Lin, P.; Colina, C. M. Molecular Insight into the ProteinPolymer Interactions in N-Terminal PEGylated Bovine Serum Albumin. *J. Phys. Chem. B* **2019**, *123* (25), 5196−5205.
(42) Munasinghe, A.; Mathavan, A.; Mathavan, A.; Lin, P.; Colina, C. M. PEGylation within a Confined Hydrophobic Cavity of a Protein. *Phys. Chem. Chem. Phys.* **2019**, *21* (46), 25584−25596.
(43) Yang, C.; Lu, D.; Liu, Z. How PEGylation Enhances the Stability and Potency of Insulin: A Molecular Dynamics Simulation. *Biochemistry* **2011**, *50* (13), 2585−2593.
(44) Aramini, J. M.; Tubbs, J. L.; Kanugula, S.; Rossi, P.; Ertekin, A.; Maglaqui, M.; Hamilton, K.; Ciccosanti, C. T.; Jiang, M.; Xiao, R.; Soong, T. T.; Rost, B.; Acton, T. B.; Everett, J. K.; Pegg, A. E.; Tainer, J. A.; Montelione, G. T. Structural Basis of O6-Alkylguanine Recognition by a Bacterial Alkyltransferase-like DNA Repair Protein. *J. Biol. Chem.* **2010**, *285* (18), 13736−13741.
(45) Rossi, P.; Swapna, G. V. T.; Huang, Y. J.; Aramini, J. M.; Anklin, C.; Conover, K.; Hamilton, K.; Xiao, R.; Acton, T. B.; Ertekin, A.; Everett, J. K.; Montelione, G. T. A Microscale Protein NMR Sample Screening Pipeline. *Journal of Biomolecular NMR* **2010**, *46*, 11−22.
(46) Ghosh, A.; Ostrander, J. S.; Zanni, M. T. Watching Proteins Wiggle: Mapping Structures with Two-Dimensional Infrared Spectroscopy. *Chem. Rev.* **2017**, *117* (16), 10726.
(47) Valentine, M. L.; Al-Mualem, Z. A.; Baiz, C. R. Pump Slice Amplitudes: A Simple and Robust Method for Connecting Two-Dimensional Infrared and Fourier Transform Infrared Spectra. *J. Phys. Chem. A* **2021**, *125* (29), 6498−6504.
(48) Chen, X.; Roeters, S. J.; Cavanna, F.; Alvarado, J.; Baiz, C. R. Crowding Alters F-Actin Secondary Structure and Hydration. *Commun. Biol.* **2023**, *6* (1), 900.
(49) Kwak, K.; Rosenfeld, D. E.; Fayer, M. D. Taking Apart the Two-Dimensional Infrared Vibrational Echo Spectra: More Information and Elimination of Distortions. *J. Chem. Phys.* **2008**, *128* (20), 204505.
(50) Fayer, M. D. Dynamics of Liquids, Molecules, and Proteins Measured with Ultrafast 2D IR Vibrational Echo Chemical Exchange Spectroscopy. *Annu. Rev. Phys. Chem.* **2009**, *60*, 21−38.
(51) Park, S.; Kwak, K.; Fayer, M. D. Ultrafast 2D-IR Vibrational Echo Spectroscopy: A Probe of Molecular Dynamics. *Laser Phys. Lett.* **2007**, *4* (10), 704−718.
(52) la Cour Jansen, T.; Dijkstra, A. G.; Watson, T. M.; Hirst, J. D.; Knoester, J. Modeling the Amide I Bands of Small Peptides. *J. Chem. Phys.* **2006**, *125* (4), No. 044312.
(53) Hamm, P.; Woutersen, S. Coupling of the Amide Modes of the Glycine Dipeptide Coupling of the Amide Modes; **2002**; Vol. 75.

https://doi.org/10.1021/jacsau.5c01692
JACS Au 2026, 6, 1801−1811

(54) Schmidt, J. R.; Corcelli, S. A.; Skinner, J. L. Ultrafast Vibrational Spectroscopy of Water and Aqueous N-Methylacetamide: Comparison of Different Electronic Structure/Molecular Dynamics Approaches. *J. Chem. Phys.* **2004**, *121* (18), 8887−8896.
(55) Pritzlaff, A.; Ferré, G.; Dargassies, E.; Williams, C. O.; Gonzalez, D. D.; Eddy, M. T. Conserved Protein-Polymer Interactions across Structurally Diverse Polymers Underlie Alterations to Protein Thermal Unfolding. *ACS Cent. Sci.* **2023**, *9* (4), 685.
(56) Eaves, J. D.; Tokmakoff, A.; Geissler, P. L. Electric Field Fluctuations Drive Vibrational Dephasing in Water. *J. Phys. Chem. A* **2005**, *109* (42), 9424−9436.
(57) Stevenson, P.; Tokmakoff, A. Ultrafast Fluctuations of High Amplitude Electric Fields in Lipid Membranes. *J. Am. Chem. Soc.* **2017**, *139* (13), 4743−4752.
(58) Rodríguez-Martínez, J. A.; Solá, R. J.; Castillo, B.; Cintrón-Colón, H. R.; Rivera-Rivera, I.; Barletta, G.; Griebenow, K. Stabilization of α-Chymotrypsin upon PEGylation Correlates with Reduced Structural Dynamics. *Biotechnol. Bioeng.* **2008**, *101* (6), 1142.

https://doi.org/10.1021/jacsau.5c01692
JACS Au 2026, 6, 1801−1811